A&A 614, L2 (2018)
https://doi.org/10.1051/0004-6361/201833363

Astronomy & Astrophysics

LETTER TO THE EDITOR

Cosmic dance at $z \sim 3$: Detecting the host galaxies of the dual AGN system LBQS 0302−0019 and *Jil* with HAWK-I+GRAAL⋆

B. Husemann[1], R. Bielby[2], K. Jahnke[1], F. Arrigoni-Battaia[3], G. Worseck[4], T. Shanks[2], J. Wardlow[2], and J. Scholtz[2]

[1] Max Planck Institute for Astronomy, Königstuhl 17, 69117 Heidelberg, Germany
e-mail: husemann@mpia-hd.mpg.de
[2] Centre for Extragalactic Astronomy, Durham University, South Road, Durham, DH1 3LE, UK
[3] European Southern Observatory, Karl-Schwarzschild-Str. 2, 85748 Garching bei München, Germany
[4] Institut für Physik und Astronomie, Universität Potsdam, Karl-Liebknecht-Str. 24/25, 14476 Potsdam, Germany

Received 4 May 2018 / Accepted 23 May 2018

ABSTRACT

We recently discovered that the luminous radio-quiet quasi-stellar objects (QSO) LBQS 0302−0019 at $z = 3.286$ is likely accompanied by an obscured AGN at 20 kpc projected distance, which we dubbed *Jil*. It represents the tightest candidate system of an obscured and unobscured dual AGN at $z > 3$. To verify the dual AGN scenario, we obtained deep K_s band (rest-frame V band) imaging with the VLT/HAWK-I+GRAAL instrument at 0.″4 resolution during science verification in January 2018. We detect the individual host galaxies of the QSO and *Jil* with estimated stellar masses of $\log(M_\star/M_\odot) = 11.4 \pm 0.5$ and $\log(M_\star/M_\odot) = 0.9 \pm 0.5$, respectively. Near-IR spectra obtained with Very Large Telescope-K-band Multi Object Spectrograph (VLT-KMOS) reveal a clear [O III] λ5007 line detection at the location of *Jil* that does not contribute significantly to the K_s band flux. Both observations therefore corroborate the dual AGN scenario. A comparison to Illustris simulations suggests a parent halo mass of $\log(M_{\rm halo}/M_\odot) = 13.2 \pm 0.5$ for this interacting galaxy system, corresponding to a massive dark matter halo at that epoch.

Key words. Galaxies: interactions – Galaxies: high-redshift – large-scale structure of Universe – instrumentation: adaptive optics – quasars: individual: LBQS 0302−0018

1. Introduction

Major mergers were initially thought to be one of the main triggering mechanisms for luminous quasi-stellar objects (QSO, e.g., Sanders et al. 1988; Canalizo & Stockton 2001; Hopkins et al. 2005). While major mergers certainly promote gas fueling toward the centers of galaxies in merging systems (e.g., Di Matteo et al. 2005; Springel et al. 2005), it is currently heavily debated whether this is really the dominant mode for fueling supermassive black holes (SMBHs) and triggering the most luminous QSOs (e.g., Cisternas et al. 2011; Kocevski et al. 2012; Mechtley et al. 2016). For QSOs at $z > 6$, a [C II] survey with ALMA revealed that luminous QSOs exhibit an excess in the number counts of massive companion galaxies within <100 kpc (Decarli et al. 2017), suggesting that dense environments and interactions might play an important role in the rapid evolution of the first SMBH systems in the Universe. However, for these systems, only one of the expected SMBHs in the merging galaxies is usually seen to be active.

Recently, we discovered with MUSE at the Very Large Telescope (VLT) that the luminous radio-quiet QSO LBQS 0302−0019 is accompanied by a luminous He II emitter, dubbed *Jil*, about 2.″9 (20 kpc) away (Husemann et al. 2018). The emission of *Jil* is best explained by an embedded obscured active galactic nucleus (AGN), so that the system represents the tightest pair of an unobscured and obscured AGN at $z > 3$. Frey & Gabányi (2018) analyzed archival Very Large Array radio images that revealed radio emission at the location of LBQS 0302−0019, but not at the position of *Jil*. This agrees with the expected AGN luminosity ratio at the depth of the radio data. The current radio data therefore do not provide additional constraints on the nature of *Jil,* and high-resolution X-ray observations with *Chandra* have not been obtained so far.

In this Letter we present K-band spectroscopy and adaptive-optics assisted imaging confirming the presence of a massive host galaxy at the location of *Jil* as a necessary requirement for the dual AGN scenario. Furthermore, we estimate the associated halo mass of this system based on one of the current hydrodynamical numerical simulations.

We adopt a flat cosmology with $\Omega_{\rm m} = 0.3$, $\Omega_\Lambda = 0.7$, and $H_0 = 70\,{\rm km\,s^{-1}\,Mpc^{-1}}$. The physical scale at $z = 3.286$ is 7.48 kpc arcsec^{-1} and magnitudes are given in the Vega system.

2. Observations and data reduction

2.1. VLT/HAWK-I+GRAAL K_s-band imaging

We targeted this dual AGN system during the science verification (SV) with the GRound-layer Adaptive optics Assisted by Laser instrument (GRAAL, Paufique et al. 2010), which provides a seeing enhancer for the wide-field near-infrared imager HAWK-I (Casali et al. 2006) at the VLT. HAWK-I covers a 7.′5 × 7.′5 field of view (FoV) using an array of 2 × 2 Hawaii-2RG

⋆ Based on observations collected at the European Organisation for Astronomical Research in the Southern Hemisphere under ESO programme(s) 60.A-9471(A) and 100.A-0134(B).

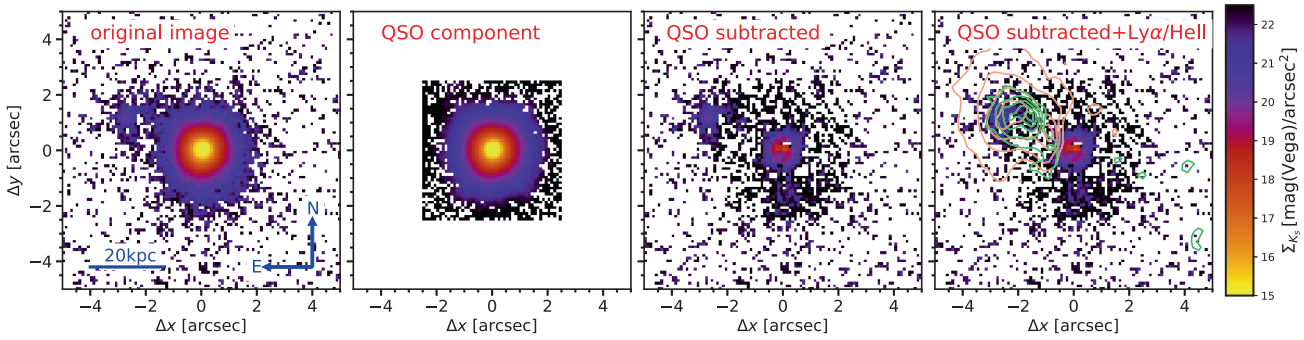

Fig. 1. K_s-band image from VLT/HAWK-I of LBQS 0302−0019 and *Jil* with a spatial resolution of 0.″4 (FWHM). From left to right, we present *panel a*) the original K_s-band image, *panel b*) the PSF taken from a nearby star properly scaled to the QSO based on the best-fit GALFIT model, *panel c*) the residual image after QSO component subtraction, and *panel d*) the residual image with overplotted Lyα contours (*red*) at $0.2, 0.4, 0.6, 0.8 \times 10^{-16}$ erg s^{-1}cm^{-2} arcsec^{-2} and He II λ1640 contours (*green*) at $0.4, 0.6, 0.8, 1.0$, and 1.2×10^{-17} erg s^{-1} cm^{-2} arcsec^{-2} from the VLT-MUSE observations (Husemann et al. 2018) with a spatial resolution of 1″ (FWHM). Strong PSF residuals from the QSO in the Lyα and He II contours have been masked out for clarity.

detectors with a 15″ gap between the four quadrants. We observed LBQS 0302−0019 in the K_s band during the SV run from 2–5 January 2018. The observations were split into two separate observing blocks consisting of 12 dithered pointings with 20×10 s exposures each. The QSO was centered in quadrants 1 and 3 of the detector array in the respective observing blocks, which amounts to 4800 s on source exposure time.

The data were reduced with the standard ESO pipeline for HAWK-I. The photometric zero-point for the combined image was determined through aperture photometry of two bright 2MASS stars in the common field of the two pointings. We consider that the photometric zero-point ($m_{K_s,0} = 22.73$ mag) estimated in this way has an intrinsic uncertainty of 0.1 mag. An image cutout of the dual AGN system region is shown in Fig. 1 and clearly reveals a prominent continuum source exactly at the expected location of *Jil* at a spatial resolution of 0.″4 (FWHM).

2.2. KMOS near-IR integral-field spectroscopy

We also observed the dual AGN system with the K-band Multi Object Spectrograph (KMOS, Sharples et al. 2013). The KMOS data were taken on 27 January 2018 as part of a back-up program of the VLT LBG Redshift Survey (VLRS; Bielby et al. 2013, 2017), intended to fill gaps in the guaranteed observing time that are due to pointing restrictions, sub-optimal sky conditions, and gaps in the distribution of primary target fields on the sky.

KMOS is a near-IR multi-object integral field unit (IFU) instrument mounted on VLT UT4. It consists of 24 individual 2.″8 × 2.″8 IFUs (with pixel scales of 0.″2). Only two IFUs were used to cover the dual AGN system. For these observations, KMOS was operated with the HK grism in place, providing wavelength coverage from 1.484 μm to 2.442 μm, with a spectral resolution ranging from $R \sim 1500$ to $R \sim 2500$ correspondingly.

Observations were taken in nod-to-sky mode with an ABAABAAB pattern, where A and B represent the two nod positions. Given the proximity of *Jil* to LBQS 0302−0019, we were unable to place IFUs on the two targets simultaneously, and so *Jil* was targeted during nod position B, and LBQS 0302−0019 was targeted in position A. In both cases, the IFUs nodded to selected empty sky locations in their respective "off" nod positions, to aid sky removal from the science exposures. The two IFUs were positioned to provide some overlap in their coverage, resulting in overlaps of ≈0.″8 in R.A. and ≈1.″8 in declination. Each nod was observed for 600s, leading to integration times on LBQS 0302−0019 and *Jil* of 3000s and 1800s, respectively.

The data were reduced using ESOREX with the standard ESO pipeline recipes (Davies et al. 2013), incorporating dark and flat frame subtraction, wavelength calibration, illumination correction, standard star flux calibration, and the overall processing and stacking. The final image quality of the cube is 0.″65 (FWHM). We used the KMOS SKY-TWEAK routine to optimally remove the near-IR sky lines and applied the Zurich Atmosphere Purge (ZAP; Soto et al. 2016) code on the final cube to further suppress sky line residuals.

3. Results

3.1. QSO subtraction

Given the brightness of the QSO LBQS 0302−0019, it is crucial to subtract the QSO light to properly resolve the host galaxies of the QSO and *Jil* in the HAWK-I data. To estimate the QSO contribution, we first created an empirical point-spread function (PSF) from the nearby star 2MASS J03044733−0007499 ($m_{K_s} = 13.46 \pm 0.04$ mag), which is just 40″ away from the QSO. In a second step, we used GALFIT (v3, Peng et al. 2010) to model the data as a superposition of a single Sersić profile for each of the two galaxies and a point source for the QSO. During the fitting, we fixed the Sersić index to $n = 1$ to avoid nonphysically large indices, which are caused by the extreme brightness ratio for the QSO host galaxy and the low spatial resolution of 2.8 kpc (FWHM) compared to the expected galaxy size. The resulting model and QSO subtracted image are shown in Fig. 1, from which we infer $m_{K_s} = 19.2 \pm 0.1$ mag for the QSO host galaxy and $m_{K_s} = 20.6 \pm 0.2$ mag for *Jil*.

3.2. Host morphology

The HAWK-I K_s image (Fig. 1c) reveals that the host galaxy of *Jil* appears asymmetric in the rest-frame V band with a faint extension toward the west side. It is unclear at the given spatial resolution and depth whether *Jil* is one distorted galaxy or itself a merger of two galaxies. In comparison, the bright knot in the H I Lyα nebula recovered with MUSE is centered on *Jil* (Fig. 1d) and traces its morphology well, considering that the resolution is more than twice lower. The same applies to the He II λ1640 Å

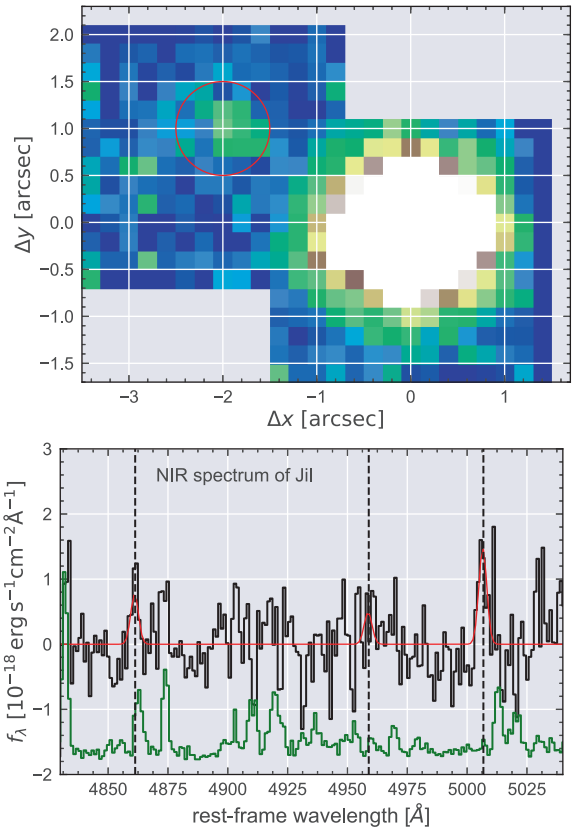

Fig. 2. *Upper panel*: Narrow-band image (25 Å wide in the observed frame) centered on the redshifted [O III] λ5007 extracted from the KMOS datacube. The QSO dominates the emission, but a weak source is detected at the location of *Jil*. *Lower panel:* Aperture spectrum (black line) within 0.″5 radius centered on *Jil* zoomed-in to the wavelength range covering the redshifted Hβ and [O III] $\lambda\lambda$4960, 5007 lines (vertical dashed lines). The green line represent the error spectrum (offset by -2×10^{-18} for readability) to highlight the position of sky lines. The best-fit model with a fixed [O III] doublet ratio is shown as the red line.

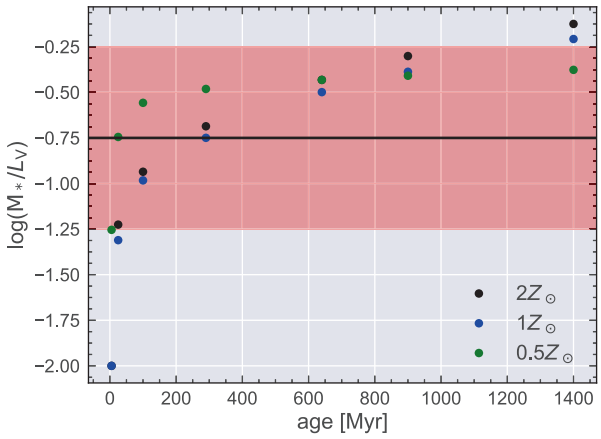

Fig. 3. Rest-frame V band mass-to-light ratio as a function of stellar population age for three metallicities. For our purpose, we adopt a mean mass-to-light ratio of $\log(M_\star/L_V) = -0.75$ (black line) with an uncertainty of ±0.5 dex (red shaded band).

emission, but it is more compact and shows a slight preference to the peak shortly west of *Jil*. The clear matching of the highly ionized gas with the presence of a distinct galaxy at the location of *Jil* is consistent with the picture of an obscured AGN at its center, but it is not a clear proof for the AGN presence as such.

3.3. Rest-frame optical nebular emission

From the KMOS data we reconstructed an [O III] λ5007 narrow-band image at the redshift of the system (Fig. 2). In addition to the bright emission from the QSO, we detect also faint [O III] emission with 5σ significance at the location of *Jil,* as expected for an obscured AGN. The observed line flux is $f_{[O\,III]} = (2.5\pm0.5)\times10^{-17}$ erg cm^{-2} s^{-1} corresponding to $L_{[O\,III]} = (2.4\pm0.5)\times10^{42}$ erg s^{-1}. With the conversion factor of $L_{bol}/L_{[O\,III]} \approx 3500$ from Heckman et al. (2004), we estimate a bolometric luminosity for *Jil* of $L_{bol}\sim4.4\times10^{45}$ erg s^{-1} with a systematic uncertainty of 0.4 dex due to the scatter in the relation.

Compared to the bolometric luminosity of $L_{bol} = 1\times10^{48}$ erg s^{-1} for LBQS 0302−0019 (Shen 2016), the [O III]-based luminosity of *Jil* is a factor of 100–620 lower. This is slightly higher than our constraints from the He II photoionization models (Husemann et al. 2018), which required a minimum luminosity of a factor 600–1000 fainter than LBQS 0302−0018, assuming a distance of 100 pc of the ionized gas clouds to the obscured AGN. This discrepancy can be easily explained either by a larger distance of the gas clouds from the AGN, or by the effect of dust extinction on the He II emission line.

We cannot detect any other emission lines such as [O III] λ4960, Hβ, or [O II] $\lambda\lambda$3726, 3729 at the location of *Jil* in the shallow KMOS data. Since [O III] λ5007 is the brightest line in case of AGN ionization, we expect non-detections for all other lines given the signal-to-noise ratio (S/N) of our data. To estimate the emission-line contribution to the HAWK-I broad-band observations, we assumed an [O III] doublet line ratio of 3 (Storey & Zeippen 2000) and ([O III] λ5007)/H$\beta\sim10$ to create a mock emission-line spectrum for the K_s band. This leads to an expected pure emission-line brightness of $m_{K_s} = 29$ mag (Vega), confirming that contributions from lines can be safely neglected in the HAWK-I K_s band.

3.4. Stellar masses and halo mass

At $z = 3.3$, the age of the Universe was about 1.8 Gyr, which sets a hard boundary for the age of the stellar population. However, the rest-frame V band mass-to-light ratio is still changing by an order of magnitude within the possible range in ages from 100 Myr to 1.8 Gyr and metallicity (Fig. 3), based on the Bruzual & Charlot (2003) stellar population models and assuming a Chabrier initial mass function. While the far-UV line diagnostics imply sub-solar metallicity (Husemann et al. 2018), we adopt a mean mass-to-light ratio of $\log(M_\star/L_V) = -0.75\pm0.5$ to be conservative, which leads to stellar masses of $\log(M_\star/M_\odot) = 11.4\pm0.5$ and $\log(M_\star/M_\odot) = 10.9\pm0.5$ for the QSO host and *Jil*, respectively. The uncertainties in the stellar masses are entirely dominated by the uncertainty in the stellar age and the corresponding mass-to-light ratio rather than photometric errors. Given a BH mass of $M_{BH} = 2.3\times10^9\,M_\odot$ (Shen 2016), the inferred host galaxy mass of the QSO is fully consistent with the high-z M_{BH}–$M_\star$ relation (e.g., Jahnke et al. 2009).

To place this system in perspective, we considered the dark matter halo distribution from the Illustris simulation (Vogelsberger et al. 2014), covering a comoving volume of 106.5 Mpc^3. We selected halos containing a close pair (<50 kpc) of sub-halos containing stellar masses of $\log(M_\star/M_\odot) > 9.0$ and stellar mass ratios $M_1/M_2 < 10$. At $z\sim3.3$, the Illustris catalog contains 21 such systems (Fig. 4), but none at the total stellar

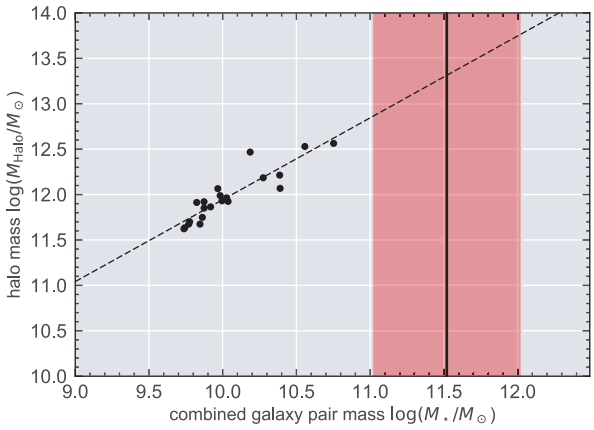

Fig. 4. Parent halo mass as a function of total stellar mass at $z \sim 3.3$ from the Illustris simulation (Vogelsberger et al. 2014) for nearly equal mass $M_1/M_2 < 10$ galaxy pairs with a separation smaller than 50 kpc. The position of our dual AGN pair system is indicated by the vertical black line, with uncertainties highlighted by the red shaded area. There is no similar system in Illustris due to the limited volume (106.5 Mpc^3 comoving), but the extrapolation from lower masses (dashed line) implies a parent halo mass of $12.8 < \log(M_{\rm halo}/M_\odot) < 13.7$.

mass we estimated for our dual AGN system. We therefore fit the halo mass as a function of the combined stellar mass with a power law to extrapolate the observed trend to higher masses. Given the combined stellar mass for the QSO and *Jil,* we find a range in halo masses of $12.8 < \log(M_{\rm halo}/M_\odot) < 13.7$, which corresponds to a very massive dark matter halo at that redshift based on predicted halo mass functions (e.g., Watson et al. 2013).

4. Discussion

Luminous QSOs at high redshifts are thought to be associated with massive dark matter halos and dense environments because a rapid BH growth at early cosmic epoch is required. Observational evidence of overdensities around high-redshift luminous QSOs has been established in several ways. Luminous radio-loud AGN at $1.2 < z < 3$ have been found to systematically reside in galaxy overdensities on arcminute scales (e.g., Ivison et al. 2000; Smail et al. 2003; Wylezalek et al. 2013; Rigby et al. 2014; Malavasi et al. 2015; Jones et al. 2015; Silva et al. 2015). Similar studies for radio-quiet AGN have also revealed galaxy overdensities around them (e.g., Utsumi et al. 2010; Capak et al. 2011; Morselli et al. 2014; Jones et al. 2017), although contradictory results have been reported (Kikuta et al. 2017; Mazzucchelli et al. 2017). Furthermore, halo masses of luminous AGN have been estimated through clustering studies, which either found that they reside in overdensities (e.g., Croom et al. 2002; Coil et al. 2009) or in normal environments (Coil et al. 2007). The inconsistencies may be related to the intrinsic properties of QSOs as BH mass has been suggested to correlate most strongly with the halo mass (e.g., Krumpe et al. 2015) or that different galaxy populations, such as Lyα emitters, Lyman-break galaxies, or dusty galaxies, are considered for the clustering analysis. Nevertheless, recent clustering measurements of AGN in the COSMOS field yield a typical halo mass of $\sim 10^{13}\ M_\odot$ at $z \sim 3$ (Allevato et al. 2016), in agreement with our results.

Other works focused on the local environment around luminous QSOs. Here, it is striking to see that luminous QSOs reveal an excess in the number counts of massive star-forming galaxies in their vicinity at $z > 6$ (Decarli et al. 2017) and $z \sim 4.8$ (Trakhtenbrot et al. 2017). This is in agreement with the notion of a strongly clustered galaxy environment around QSOs at high redshifts (e.g., García-Vergara et al. 2017) and an excess of unobscured dual AGN with <40 kpc separations (Hennawi et al. 2006). Although the AGN environment is certainly significantly evolving with redshift, luminous AGN, such as LBQS 0302−0019, may be signposts of the most vigorous evolution of galaxies in overdensities at early epochs.

5. Conclusion

Based on deep K-band spectroscopy with KMOS and high-resolution imaging with HAWK-I+GRAAL, we have identified the massive ($\log(M_\star/M_\odot) = 10.9 \pm 0.5$) host galaxy of *Jil*, the obscured companion AGN to LBQS0302−0019 at a projected separation of about 20 kpc. This clearly supports the obscured AGN nature of *Jil* since the presence of a massive host galaxy implies the existence of a super-massive black hole, potentially powering an AGN. Hence, we expect a direct detection of AGN engine signatures from *Jil* in the radio (core emission), mid-IR (torus) or X-rays (disk corona) with sufficiently deep observations.

The combined stellar mass of both galaxies suggests a very massive parent halo of this intriguing dual AGN system. This is in agreement with observations of the environment around luminous AGN comparable to LBQS 0302−0019 at similar or even higher redshifts. It suggests that these luminous AGN are part of and shaped by a vigorous evolutionary phase that might be important to set the properties of massive present-day galaxies.

Acknowledgements. We thank the anonymous referee for a fast and constructive review. We particularly thank A. van der Wel for helpful discussion about high-redshift galaxy properties, and A. Pillepich for an introduction to the Illustris simulations data. RMB, TS, and JWL acknowledge the Science and Technology Facilities Council (STFC; grant ST/P000541/1) for support. JLW acknowledges support from an STFC Ernest Rutherford Fellowship (ST/P004784/1). We also thank A. Tiley for facilitating our KMOS observations.

References

Allevato, V., Civano, F., Finoguenov, A., et al. 2016, ApJ, 832, 70
Bielby, R., Hill, M. D., Shanks, T., et al. 2013, MNRAS, 430, 425
Bielby, R. M., Shanks, T., Crighton, N. H. M., et al. 2017, MNRAS, 471, 2174
Bruzual, G., & Charlot, S. 2003, MNRAS, 344, 1000
Canalizo, G. & Stockton, A. 2001, ApJ, 555, 719
Capak, P. L., Riechers, D., Scoville, N. Z., et al. 2011, Nature, 470, 233
Casali, M., Pirard, J.-F., Kissler-Patig, M., et al. 2006, in Proc. SPIE, 6269, 62690W
Cisternas, M., Jahnke, K., Inskip, K. J., et al. 2011, ApJ, 726, 57
Coil, A. L., Hennawi, J. F., Newman, J. A., Cooper, M. C., & Davis, M. 2007, ApJ, 654, 115
Coil, A. L., Georgakakis, A., Newman, J. A., et al. 2009, ApJ, 701, 1484
Croom, S. M., Boyle, B. J., Loaring, N. S., et al. 2002, MNRAS, 335, 459
Davies, R. I., Agudo Berbel, A., Wiezorrek, E., et al. 2013, A&A, 558, A56
Decarli, R., Walter, F., Venemans, B. P., et al. 2017, Nature, 545, 457
Di Matteo, T., Springel, V., & Hernquist, L. 2005, Nature, 433, 604
Frey, S. & Gabányi, K. É. 2018, Res. Notes AAS, 2, 49
García-Vergara, C., Hennawi, J. F., Barrientos, L. F., & Rix, H.-W. 2017, ApJ, 848, 7
Heckman, T. M., Kauffmann, G., Brinchmann, J., et al. 2004, ApJ, 613, 109
Hennawi, J. F., Strauss, M. A., Oguri, M., et al. 2006, AJ, 131, 1
Hopkins, P. F., Hernquist, L., Cox, T. J., et al. 2005, ApJ, 630, 705
Husemann, B., Worseck, G., Arrigoni Battaia, F., & Shanks, T. 2018, A&A, 610, L7
Ivison, R. J., Dunlop, J. S., Smail, I., et al. 2000, ApJ, 542, 27
Jahnke, K., Bongiorno, A., Brusa, M., et al. 2009, ApJ, 706, L215
Jones, S. F., Blain, A. W., Lonsdale, C., et al. 2015, MNRAS, 448, 3325
Jones, S. F., Blain, A. W., Assef, R. J., et al. 2017, MNRAS, 469, 4565
Kikuta, S., Imanishi, M., Matsuoka, Y., et al. 2017, ApJ, 841, 128

Kocevski, D. D., Faber, S. M., Mozena, M., et al. 2012, ApJ, 744, 148
Krumpe, M., Miyaji, T., Husemann, B., et al. 2015, ApJ, 815, 21
Malavasi, N., Bardelli, S., Ciliegi, P., et al. 2015, A&A, 576, A101
Mazzucchelli, C., Bañados, E., Decarli, R., et al. 2017, ApJ, 834, 83
Mechtley, M., Jahnke, K., Windhorst, R. A., et al. 2016, ApJ, 830, 156
Morselli, L., Mignoli, M., Gilli, R., et al. 2014, A&A, 568, A1
Paufique, J., Bruton, A., Glindemann, A., et al. 2010, in Proc. SPIE, 7736, 77361P
Peng, C. Y., Ho, L. C., Impey, C. D., & Rix, H. 2010, AJ, 139, 2097
Rigby, E. E., Hatch, N. A., Röttgering, H. J. A., et al. 2014, MNRAS, 437, 1882
Sanders, D. B., Soifer, B. T., Elias, J. H., Neugebauer, G., & Matthews, K. 1988, ApJ, 328, L35
Sharples, R., Bender, R., Agudo Berbel, A., et al. 2013, The Messenger, 151, 21
Shen, Y. 2016, ApJ, 817, 55
Silva, A., Sajina, A., Lonsdale, C., & Lacy, M. 2015, ApJ, 806, L25
Smail, I., Scharf, C. A., Ivison, R. J., et al. 2003, ApJ, 599, 86
Soto, K. T., Lilly, S. J., Bacon, R., Richard, J., & Conseil, S. 2016, MNRAS, 458, 3210
Springel, V., Di Matteo, T., & Hernquist, L. 2005, ApJ, 620, L79
Storey, P. J. & Zeippen, C. J. 2000, MNRAS, 312, 813
Trakhtenbrot, B., Lira, P., Netzer, H., et al. 2017, ApJ, 836, 8
Utsumi, Y., Goto, T., Kashikawa, N., et al. 2010, ApJ, 721, 1680
Vogelsberger, M., Genel, S., Springel, V., et al. 2014, Nature, 509, 177
Watson, W. A., Iliev, I. T., D'Aloisio, A., et al. 2013, MNRAS, 433, 1230
Wylezalek, D., Galametz, A., Stern, D., et al. 2013, ApJ, 769, 79